Three-dimensional mesoscopic modeling of equiaxed dendritic solidification in a thin sample: effect of convection flow

To cite this article: A. Olmedilla *et al* 2019 *IOP Conf. Ser.: Mater. Sci. Eng.* **529** 012040

IOP Conf. Series: Materials Science and Engineering **529** (2019) 012040 doi:10.1088/1757-899X/529/1/012040

Three-dimensional mesoscopic modeling of equiaxed dendritic solidification in a thin sample: effect of convection flow

A. Olmedilla[1], M. Založnik[1], M. Cisternas Fernández[1], A. Viardin[2], H. Combeau[1]

[1] Université de Lorraine, CNRS, IJL, F-54000 Nancy, France
[2] Access e.V., Intzestr. 5, D-52072 Aachen, Germany

E-mail: antonio.olmedilla.aero@gmail.com

Abstract. A 3D mesoscopic envelope model is used to numerically simulate the experimental X-ray observations of the equiaxed dendritic isothermal solidification of a thin sample of Al-20 wt%Cu alloy including the natural convection flow. Several four-grain simulations are run to investigate the effect of the convection, of the grain position, and of the grain rotation on the tip growth kinetics of one of the grains. We show that the effect of convection flow – consequence of the presence of gravity parallel to the sample thickness direction, z – on the growth kinetics of the reference grain depends significantly on the position of the grain along the sample thickness.

1. Introduction

Different approaches can be used in numerical modeling of solidification microstructures, depending on the desired simulation scale. At the microscopic scale, approaches such as the phase-field modeling [1], the pseudo front tracking [2], the enthalpy method [3], or the microscopic CA [4] can be used, whereas at a mesoscopic scale, the needle network (DNN) [5], the cellular-automaton finite-element (CAFE) model [6] and the envelope model [7, 8, 9] are available. The mesoscopic approaches achieve a less detailed description of the dendritic grain morphology compared to the microscopic approaches, but have a much smaller computational cost, i.e. larger domains can be easily simulated.

Herein we focus on the mesoscopic envelope approach, which is convenient to simulate solidification phenomena for which interactions at the scale of a group of grains are important [8]. We show that the three-dimensional mesoscopic envelope model is a useful numerical tool to describe the grain morphology in case of equiaxed dendritic solidification in thin samples used for in-situ observations of metallic alloys [10]. Additionally, we show the effect of convective flow on the growth kinetics. This effect depends on the initial grain position along the sample thickness direction, z, which is parallel to gravity, and the grain orientation, more precisely, the misalignment of the grain preferential growth directions $\langle 100 \rangle$ with respect to the direction z.

2. Mesoscopic Envelope Model

We use the in-house mesoscopic envelope computer code CrystalFOAM. In the mesoscopic envelope model the complex dendritic grain morphology is approximated as an envelope [7].

For an alloy under the assumption of a homogeneous temperature field, the growth of the dendrite tips is governed by the solute flux that the tips eject to the liquid. The Ivantsov analytical tip growth solution [11] is employed in a stagnant film formulation [12] to relate the tip growth Peclet number, Pe_{tip}, to the supersaturation, Ω_δ, at a finite distance, δ, from the tip. The Peclet number is defined by $Pe_{tip} = R_{tip}V_{tip}/(2D_l)$ where R_{tip} is the tip radius, V_{tip} is tip growth velocity, and D_l is the solute diffusion coefficient in the melt. The supersaturation is defined by $\Omega_\delta = (C_l^* - C_l^\delta)/((1-k_p)C_l^*)$ where C_l^* is the liquidus equilibrium solute concentration, C_l^δ is the solute concentration in the liquid at the distance δ from the tip, and k_p is the alloy partition coefficient.

The tip velocity is obtained from Pe_{tip} by a tip selection criterion that reads $V_{tip} = 4\sigma^* D_l Pe_{tip}^2/d_o$, where $d_o = \Gamma/(m_l C_l^*(k_p-1))$ is the capillary length, m_l is the liquidus slope, Γ is the Gibbs-Thomson coefficient, and σ^* is the selection parameter. We consider $\sigma^* = (2\pi)^{-2}$ [13].

The concentration field is obtained by means of the solute convection-diffusion equation. The phase-field sharp-interface capturing method [14] is used to track the envelope contour once the growth velocity field of the grain envelope is computed. The complete description of CrystalFOAM for purely diffusive dendritic growth (no melt flow) is available in [8, 9].

In order to account for the solutal buoyancy driven flow in presence of gravity, $\vec{g}$, a two phase solid-liquid averaging approach is adopted [15]. The interior of the envelopes is considered as a two-phase medium. The distribution of the liquid fraction in the envelopes is given by a Scheil solidification model [8] and the drag on the liquid is modeled by a permeability of the porous medium. The equations of liquid mass conservation (Eq. 1), and liquid momentum conservation (Eq. 2) are included. Herein, the solid phase is assumed immobile, therefore no equations are needed for the solid.

$$\nabla \cdot \left(g_l \left\langle \vec{v}_l \right\rangle^l \right) = 0 \tag{1}$$

$$\frac{\partial}{\partial t}\left(g_l \left\langle \vec{v}_l \right\rangle^l \right) + \nabla \cdot \left(g_l \left\langle \vec{v}_l \right\rangle^l \left\langle \vec{v}_l \right\rangle^l \right) = -g_l \nabla \tilde{p} + \nabla \cdot \left(g_l \nu_l \nabla \left\langle \vec{v}_l \right\rangle^l \right) - \frac{\nu_l g_l^2}{K} \left\langle \vec{v}_l \right\rangle^l + g_l \tilde{\rho}_l \vec{g}\,, \tag{2}$$

$$\text{where } \tilde{\rho}_l = (1 - \beta_C (C_l - C_0)) \text{ and } K = \frac{l_c^2 g_l^3}{180\,(1-g_l)^2}.$$

g_l is the liquid fraction, $\langle \vec{v}_l \rangle^l$ the liquid velocity, $\tilde{p}$ the kinematic pressure, ν_l the kinematic liquid viscosity, K the hydrodynamic permeability of the dendritic grains, l_c a characteristic length of the porous structure, and β_C the solutal volume expansion coefficient. C_0 is the initial solute concentration. Additionally, the solute conservation equation is also needed:

$$g_l \frac{\partial C_l}{\partial t} + g_l \left\langle \vec{v}_l \right\rangle^l \cdot \nabla C_l = D_l \nabla \cdot (g_l \nabla C_l) + C_l (k_p - 1) \frac{\partial g_l}{\partial t} \tag{3}$$

This equation (Eq. 3) is identical to the one in the diffusive model [9] but has an additional convection term. It gives C_l outside the envelope and g_l inside the envelope. C_l inside the envelope is equal to $C_l^* = (T - T_f)/m_l$ where T_f is the melting temperature of the solvent. All transport equations are solved with the finite-volume method with a backward Euler time stepping.

3. The cases of study

3.1. In situ experimental observations: the XRMON-SOL experiment of Murphy et al.

We have numerically simulated a small sub-domain of the experiment of isothermal equiaxed dendritic solidification in a thin sample performed by Murphy et al. [10]. In this experiment the growth of 15 equiaxed dendrites under the influence of solutal interactions was observed in situ by X-ray transmission projection imaging. Growth rates of individual grain envelopes and of dendrite tips were measured from the projected images. Murphy et al. concluded that flow

convection is negligible in this experiment, despite being performed in terrestrial conditions, since the experiment is perfomed in such a way that the 200 μm thin thickness direction, z, is parallel to gravity. Similar growth characteristics of terrestrial and microgravity conditions are shown in Ref. [16].

The experimental images do not provide information on the 3D structure of the sample, namely the position of the grains in the sample thickness and their 3D orientation. Modeling can help to identify these parameters. We therefore investigate their influence on the grain growth, using mesoscopic simulation.

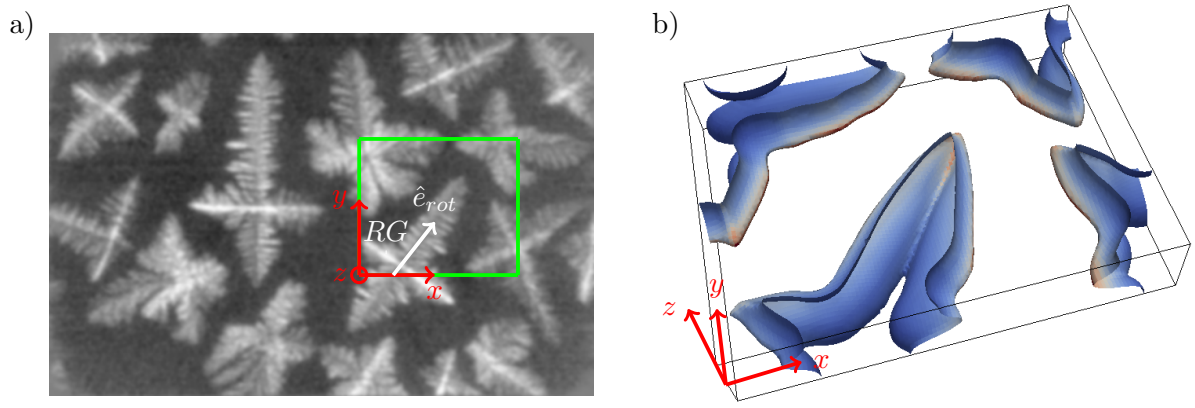

Figure 1. a) X-ray transmission projection images of growing grains from the experiment of Murphy et al. [10]. Images courtesy of D.J. Browne. b) 3D snapshot of the simulation domain and dendritic grains (RC) at the end of simulation.

3.2. Mesoscopic modeling

We establish a rectangular prismatic simulation domain of thickness equal to that of the experiment of Murphy et al. [10], $L_z = 200\,\mu$m, and length and width of $L_x = 1137.7\,\mu$m and $L_y = 883.2\,\mu$m, respectively (see Fig. 1). In the model, four grains are initialized as spherical seeds of diameter $D_{ini} = 90\,\mu$m. The nucleation time (onset of growth) is different for each of the four grains. We have used the nucleation time data available in [10]. The x and y coordinates of the seed centers are known from the experiments and are given in [10], whereas the position in the sample thickness, the coordinate z, is unknown. The grain orientation about the axes x and y is also unknown. The temperature field is assumed uniform with an initial temperature of $T_0 = 601.7°$C and a constant cooling rate of $\dot{T} = -0.05\,$K/s. A time step of 0.01 s and a uniform mesh of cubes of side $\Delta x = 10\,\mu$m are used.

The work in this paper is composed of four pairs of simulation cases. For each of these pairs, the reference grain, RG, (Fig. 1) has a different position along the sample thickness, z, and/or a different rotation about the rotation axis $\hat{e}_{rot}$ (Fig. 1). The other three grains in the simulation domain (Fig. 1b) have a vertical position of $z = 0$ (mid-thickness) and only rotations about the vertical axis, z. Each pair contains a simulation without gravity (NoGrav) and a simulation with gravity (Grav). The cases are collected in Table 1. The common thermophysical properties for the 8 different simulation cases are summarized in Table 2.

4. Simulation results and discussion

In this section we present and discuss the mesoscopic simulation results. We focus on the effect of the flow convection in each of the pairs of simulation cases (with gravity and without gravity).

Table 1. Position and rotation of the reference grain (RG) in the simulation cases.

Case Pairs	vertical position (z)	rotation about $\hat{e}_{rot}$
RC (reference case) | NoGrav / Grav	0 (mid-thickness)	0°
C30 | NoGrav / Grav	0 (mid-thickness)	30°
C100 | NoGrav / Grav	100 μm (top wall)	0°
C45+100 | NoGrav / Grav	100 μm (top wall)	45°

Table 2. Thermophysical properties used in the simulations.

Nominal concentration	C_0	20 wt%
Liquidus slope	m_l	$-3.5\,\mathrm{K/wt\%}$
Solvent melting temperature	T_f	946.37 K
Partition coefficient	k_{Cu}	0.12
Liquid diffusion coefficient	D_l	$2.8 \times 10^{-9}\,\mathrm{m^2/s}$
Gibbs-Thomson coefficient	Γ_{sl}	$2.4 \times 10^{-7}\,\mathrm{Km}$
Kinematic viscosity	ν_l	$8.43 \times 10^{-7}\,\mathrm{m^2/s}$
Solutal expansion coefficient	β_C	$-1.65 \times 10^{-2}\,\mathrm{1/wt\%}$
Char. length of the porous structure	l_c	$1.0 \times 10^{-6}\,\mathrm{m}$

We first present the results of the 3D simulation cases with gravity at the end of the growth stage ($t = 130\,\mathrm{s}$) in form of simulated projection radiographs (where the transmission is obtained with the Beer-Lambert law) that can be compared to the experimental images (see Fig. 2, left column). The difference of the RG's projected shape in the radiograph between the four cases (a-d) is basically a consequence of the position and orientation of RG. For all the pairs, the difference between the case with gravity and its homologue without gravity remains small in the radiographs, this is why only the radiographs for the gravity cases are shown.

In Fig. 2, right column, we show, for each of the gravity cases (a-d), the RG's envelope and a slice containing the center and the primary tip P1 of RG, and the vertical axis, z, at time $t = 60\,\mathrm{s}$. The colormap of the RG's envelopes refers to the normal growth velocity of the envelope, V_n, and the colormap of the slice shows the melt velocity field, U_l. The counterclockwise direction of the melt convection flow in the images is due to the higher density of the solute-enriched melt nearby the RG's tip which descends in presence of gravity. A maximum velocity of melt of approximately 30 μm/s is obtained with tip growth velocities lower than 10 μm/s for all four cases. In those cases where the primary arm grows along the sample wall the flow direction is anti-parallel to the tip growth velocity, whereas for those cases where the grain is located at mid-thickness the flow direction is perpendicular to the tip growth velocity.

Afterwards, we show quantitative results for the growth of the primary arm P1. In Fig 3a we show the length evolution of P1 over time for the four pairs of simulation cases and compare to the experiment of Murphy et al. (XRMON). All simulation cases show a trend similar to the experimental one, although the initial transient is slower in the simulations. For the cases RC and C30, the effect of gravity (convection flow) on the growth kinetics is negligible. For the cases C100 and C45+100 a more important effect of gravity is found, obtaining approximately a 10 % longer primary arm when gravity is active. The cases C100 and C45+100 with gravity give the most similar trend to that of the experiment.

In Fig 3b, we show the relative difference between the projected final area of P1 in our simulations and in the experiment Murphy et al. As before, for the cases RC and C30, the effect of gravity (convection flow) on the final area of P1 is negligible. For the cases C100 and

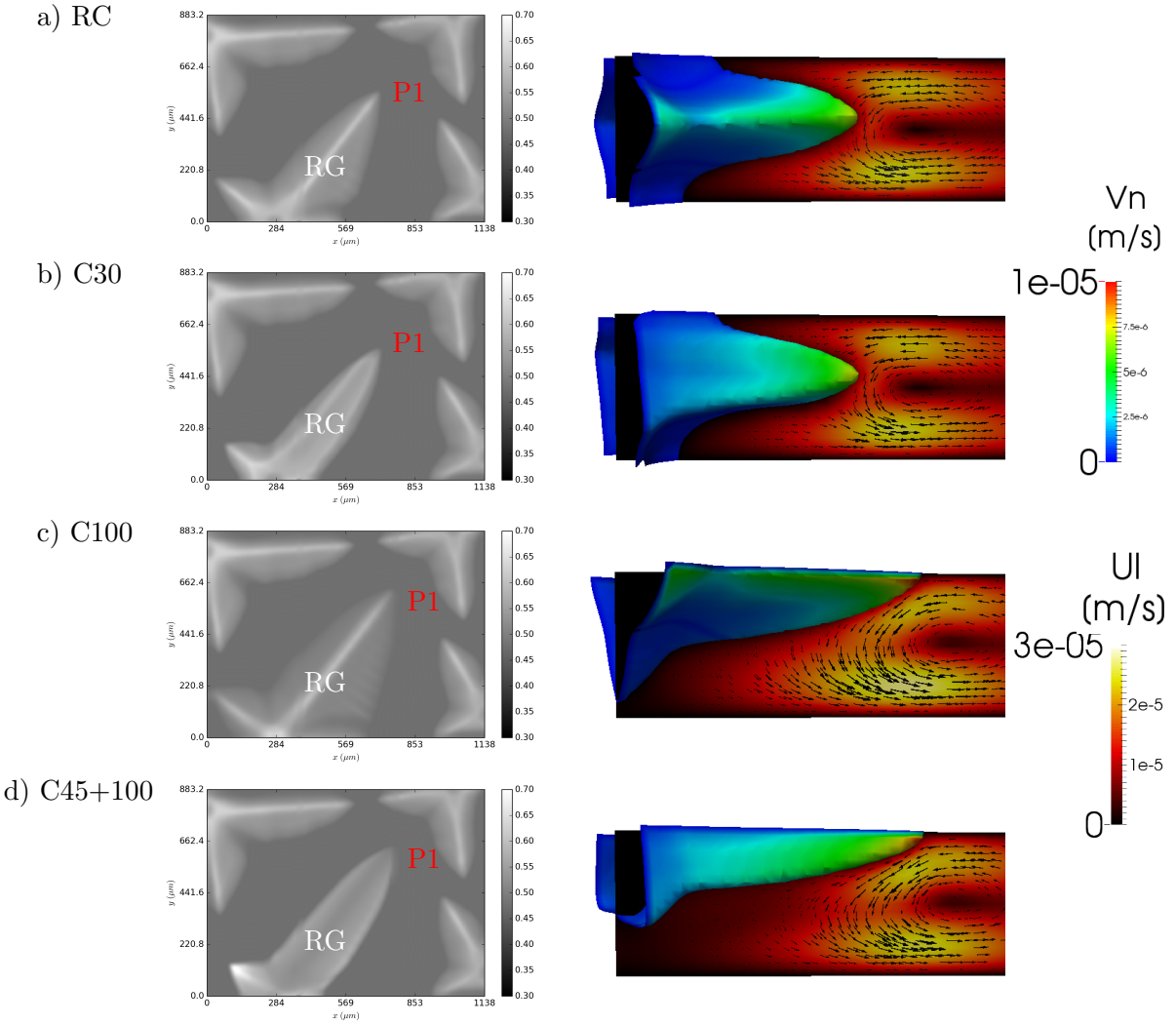

Figure 2. Left: simulation radiographs (where the grayscale represents the transmission obtained by the Beer-Lambert law) at the final instant, $t = 130\,\mathrm{s}$, for the cases: a) RC | Grav, b) C30 | Grav, c) C100 | Grav, and d) C45+100 | Grav. The reference grain is indicated in the images, RG, as well as the primary arm P1. The gray scale bar refers to the transmission coefficient. Right: RG's envelope and slice containing the center and P1 of RG and the vertical axis, z, for each of the cases a, b, c and d, at time $t = 60\,\mathrm{s}$. The normal growth velocity of the RG's envelope, V_n, and the melt velocity, U_l, are shown.

C45+100 a more important effect is found.

In this way, for cases where the vertical position of the RG's center is at the top wall (C100 and C45+100) a much important influence of the convection flow is found than for those cases where the RG's center is at the mid-thickness. This is a consequence of the higher flow of solute-depleted melt convected to the tip in cases C100 and C45+100 which increases the tip growth speed.

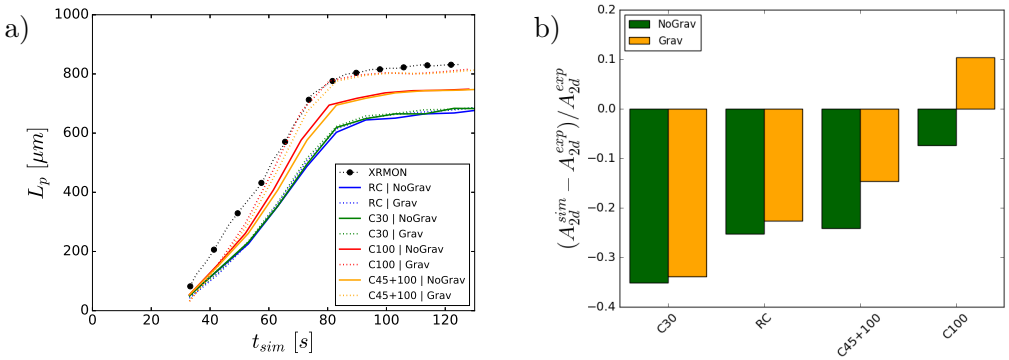

Figure 3. a) Length evolution of the primary arm P1 over time for the simulation cases RC, C30, C100, C45+100, with and without gravity, and the experiment (XRMON) of Murphy et al. (with gravity). b) Relative difference between the projected final area of P1 in the simulation cases and the experiment of Murphy et al. [10].

5. Conclusions

The mesoscopic envelope model is shown to be an useful tool to numerically simulate the equiaxed dendritic isothermal solidification including the convection flow. In case of isothermal solidification of a thin sample of Al-20 wt%Cu, we show that the effect of the thermo-solutal convection flow – consequence of the presence of gravity parallel to the sample thin thickness direction – on the growth kinetics of the reference grain depends on its initial grain position along the sample thickness.

Acknowledgments

This work was supported by the French State through the program "Investment in the future" operated by the National Research Agency (ANR) and referenced by ANR-11 LABX-0008-01 (LabEx DAMAS). We thank David J. Browne, Henri Nguyen Thi and Guillaume Reinhart for helpful discussions.

References

[1] Boukellal A K, Debierre J M, Reinhart G and Nguyen-Thi H 2018 *Materialia* **1** 62–69
[2] Jacot A and Rappaz M 2002 *Acta Materialia* **50** 1909 – 1926
[3] Voller V 2008 *International Journal of Heat and Mass Transfer* **51** 823 – 834
[4] Li D, Li R and Zhang P 2007 *Applied Mathematical Modelling* **31** 971 – 982
[5] Tourret D and Karma A 2016 *Acta Materialia* **120** 240 – 254
[6] Carozzani T, Digonnet H and Gandin C A 2012 *Modelling and Simulation in Materials Science and Engineering* **20**
[7] Steinbach I, Beckermann C, Kauerauf B, Li Q and Guo J 1999 *Acta Materialia* **47** 971 – 982
[8] Souhar Y, Felice V F D, Beckermann C, Combeau H and Založnik M 2016 *Computational Materials Science* **112** 304 – 317
[9] Viardin A, Založnik M, Souhar Y, Apel M and Combeau H 2017 *Acta Materialia* **122** 386 – 399
[10] Murphy A, Mathiesen R, Houltz Y, Li J, Lockowandt C, Henriksson K, Zimmermann G, Melville N and Browne D 2016 *Journal of Crystal Growth* **440** 38 – 46
[11] Ivantsov G 1947 *Dokl Akad Nauk SSSR* **58** 567 – 570
[12] Cantor B and Vogel A 1977 *Journal of Crystal Growth* **41** 109 – 123
[13] Langer J and Müller-Krumbhaar H 1978 *Acta Metallurgica* **26** 1681 – 1687
[14] Sun Y and Beckermann C 2007 *Journal of Computational Physics* **220** 626 – 653
[15] Založnik M and Combeau H 2010 *Computational Materials Science* **48** 1 – 10
[16] Murphy A, Mathiesen R, Houltz Y, Li J, Lockowandt C, Henriksson K, Melville N and Browne D 2016 *Journal of Crystal Growth* **454** 96 – 104